INTERNATIONAL JOURNAL FOR NUMERICAL METHODS IN FLUIDS, VOL. 4, 781–800 (1984)

PREDICTION OF PERIODIC BOUNDARY LAYERS

A. N. MENENDEZ* AND B. R. RAMAPRIAN†

Iowa Institute of Hydraulic Research, The University of Iowa, Iowa City, Iowa 52242, U.S.A.

SUMMARY

A relatively simple, yet efficient and accurate finite difference method is developed for the solution of the unsteady boundary layer equations for both laminar and turbulent flows. The numerical procedure is subjected to rigorous validation tests in the laminar case, comparing its predictions with exact analytical solutions, asymptotic solutions, and/or experimental results. Calculations of periodic laminar boundary layers are performed from low to very high oscillation frequencies, for small and large amplitudes, for zero as well as adverse time-mean pressure gradients, and even in the presence of significant flow reversal. The numerical method is then applied to predict a relatively simple experimental periodic turbulent boundary layer, using two well-known quasi-steady closure models. The predictions are shown to be in good agreement with the measurements, thereby demonstrating the suitability of the present numerical scheme for handling periodic turbulent boundary layers. The method is thus a useful tool for the further development of turbulence models for more complex unsteady flows.

KEY WORDS Unsteady Flows Periodic Boundary Layers Laminar Boundary Layers Turbulent Boundary Layers Finite-Difference Methods

1. INTRODUCTION

There has been increased interest in the study of unsteady flows in recent years. This is due to the relevance of this study to such varied applications as biofluid flows, missile aerodynamics, aircraft flutter, helicopter rotor blade flows, turbomachinery flows, etc. Unsteady inviscid flows and certain special cases of unsteady viscous flows have been studied and discussed very well in the classical literature. The work of Stokes[1] and Rayleigh[2] on unsteady laminar flows, the asymptotic analysis of periodic laminar boundary layers by Lighthill,[3] and the analysis of Uchida[4] on periodic laminar pipe-flow are examples of the above. The asymptotic analytical solutions for some unsteady laminar boundary layer flows have been extended by Hill and Stenning,[5] and more recently by Ackerberg and Phillips,[6] and Pedley.[7] However, the bulk of the laminar viscous flow problems and all the turbulent shear flow problems have to be handled via numerical methods only. Finite difference techniques have been widely used in the past several years for the numerical solution of steady two-dimensional laminar and turbulent boundary layers. The extension of these methods to unsteady/three-dimensional flows has been a topic of recent and continuing interest, particularly in the field of aerodynamics. The interest of the aerodynamicist these days is often in the prediction of non-stationary *turbulent* boundary layers, but any numerical

* Graduate Research Assistant
† Professor of Mechanical Engineering and Research Engineer

0271–2091/84/080781–20$02.00

Received 7 March 1983
Revised 13 May 1983

scheme developed for this purpose needs to be validated from its performance with laminar flows. This is very important because modelling criteria for unsteady turbulent flows—especially those in which the time scale of imposed unsteadiness is of the same order as the characteristic time scale of turbulence—are currently being investigated by several researchers. It is, therefore, necessary to have a numerically accurate procedure for the calculation of unsteady turbulent boundary layers so that implications of different turbulence models can be tested.

Numerical (finite difference) methods for laminar/turbulent boundary layers subjected to a periodic free-stream velocity have been developed, among others, by McCroskey and Philippe,[8] Cebeci,[9] Tsahalis and Telionis,[10] Nash and Patel,[11] Cousteix *et al.*,[12] Orlandi,[13] Orlandi and Ferziger[14] and Murphy and Prenter.[15] The turbulent boundary layer calculations have given inconclusive results when compared with some of the experimental data that became recently available. Furthermore, different calculation methods, using identical turbulence models, have sometimes given substantially different results (see Reference 15), making it very difficult to draw conclusions about the suitability of the proposed numerical procedure. This, perhaps, indicates the need to perform very rigorous tests for accuracy during the development of the method.

In this paper, a numerical procedure is developed and very rigorously checked for accuracy with several laminar flow solutions. The method is shown to perform very well even in extreme situations. It is then applied to predict a periodic turbulent boundary layer. The results are compared with experimental data.

2. THE NUMERICAL PROCEDURE

2.1. *Equations*

The incompressible, two-dimensional, unsteady, ensemble-averaged turbulent boundary layer equations are

$$\frac{\partial\langle U\rangle}{\partial x}+\frac{\partial\langle V\rangle}{\partial y}=0 \tag{1}$$

$$\frac{\partial\langle U\rangle}{\partial t}+\langle U\rangle\frac{\partial\langle U\rangle}{\partial x}+\langle V\rangle\frac{\partial\langle U\rangle}{\partial y}=-\frac{1}{\rho}\frac{\partial\langle p\rangle}{\partial x}+\nu\frac{\partial^2\langle U\rangle}{\partial y^2}-\frac{\partial}{\partial y}\langle uv\rangle \tag{2}$$

$$\frac{\partial\langle k\rangle}{\partial t}+\langle U\rangle\frac{\partial\langle k\rangle}{\partial x}+\langle V\rangle\frac{\partial\langle k\rangle}{\partial y}=\frac{\partial}{\partial y}[\langle(q^2/2+p/\rho)v\rangle]-\langle uv\rangle\frac{\partial\langle U\rangle}{\partial y}-\langle\varepsilon_1\rangle \tag{3}$$

The ensemble averaged values, denoted by the notation $\langle\ \rangle$, can be regarded as the average obtained from a number of realizations. The equations are analogous to the time-averaged Reynolds equations for steady turbulent flows, with $\langle k\rangle$ and $\langle uv\rangle$ being interpreted as the average turbulent kinetic energy and Reynolds shear stress, respectively. Also, with $\langle k\rangle=\langle uv\rangle=0$, they reduce to the laminar boundary layer equations. The initial and boundary conditions are

$$\begin{aligned}
&\langle U\rangle(x,0,t)=0, \qquad \langle V\rangle(x,0,t)=0, \qquad \langle k\rangle(x,0,t)=0\\
&\langle U\rangle(x,y,t)\to U_e(x,t) \quad \text{as} \quad y\to\infty\\
&\langle k\rangle(x,y,t)\to k_e=\text{free-stream turbulence intensity} \quad \text{as} \quad y\to\infty\\
&\langle U\rangle(x,y,0)=\phi_u(x,y), \qquad \langle k\rangle(x,y,0)=\phi_k(x,y)\\
&\langle U\rangle(x_0,y,t)=\psi_u(y,t), \qquad \langle k\rangle(x_0,y,t)=\psi_k(y,t)
\end{aligned} \tag{4}$$

where ϕ and ψ are known functions, and the edge velocity $U_e(x, t)$ is related to the pressure gradient via the inviscid flow equation

$$-\frac{1}{\rho}\frac{\partial\langle p\rangle}{\partial x}=\frac{\partial\langle U_e\rangle}{\partial t}+\langle U_e\rangle\frac{\partial\langle U_e\rangle}{\partial x} \tag{5}$$

If a suitable turbulence closure model is introduced, equations (1) to (3) can be solved, in general, starting from the given set of initial conditions at $t=0$. However, if the flow is periodic, the equations can be solved starting from arbitrary initial conditions and be expected to yield eventually (after the transient effects die down) a truly periodic solution independent of those particular conditions.

2.2. *Transformation of the equations for periodic boundary layers*

In this case of oscillatory boundary layers, the above equations are non-dimensionalized using the following dimensionless variables:

$$\begin{gathered}\tilde{x}=\omega x/U_0, \qquad \eta=y/b(x), \qquad \tilde{t}=\omega t\\ \tilde{u}=\langle U\rangle/U_0, \qquad \tilde{v}=\langle V\rangle/\omega b, \qquad \tilde{U}_e=\langle U_e\rangle/U_0\\ \tilde{k}=\langle k\rangle/u_\tau^2\end{gathered} \tag{6}$$

where $b(x)$ is a prescribed length scale that encloses the region where significant changes in flow properties are expected to occur, and $u_\tau(x)$ is a prescribed turbulent velocity scale of the order of the shear velocity.

The transformed equations in the $\tilde{x}$–η plane are:

$$\frac{\partial\tilde{u}}{\partial\tilde{x}}+\frac{\partial\tilde{v}}{\partial\eta}-\frac{\eta}{b}\frac{\mathrm{d}b}{\mathrm{d}\tilde{x}}\frac{\partial\tilde{u}}{\partial\eta}=0 \tag{7}$$

$$\frac{\partial\tilde{u}}{\partial\tilde{t}}+\tilde{u}\frac{\partial\tilde{u}}{\partial\tilde{x}}+\tilde{v}\frac{\partial\tilde{u}}{\partial\eta}-\frac{\tilde{u}\eta}{b}\frac{\mathrm{d}b}{\mathrm{d}\tilde{x}}\frac{\partial\tilde{u}}{\partial\eta}=\frac{\nu}{\omega b^2}\frac{\partial}{\partial\eta}\left(\frac{\partial\tilde{u}}{\partial\eta}\right)-\frac{1}{\omega bU_0}\frac{\partial}{\partial\eta}(\langle uv\rangle)+\tilde{F} \tag{8}$$

$$\frac{\partial\tilde{k}}{\partial\tilde{t}}+\tilde{u}\frac{\partial\tilde{k}}{\partial\tilde{x}}+\tilde{v}\frac{\partial\tilde{k}}{\partial\eta}-\frac{\tilde{u}\eta}{b}\frac{\mathrm{d}b}{\mathrm{d}\tilde{x}}\frac{\partial\tilde{k}}{\partial\eta}+\frac{2}{u_\tau}\frac{\partial u_\tau}{\partial\tilde{x}}\tilde{u}\tilde{k}=\frac{1}{\omega bu_\tau^2}\frac{\partial}{\partial\eta}[\langle(p/\rho+q^2/2)v\rangle]-\frac{U_0}{\omega bu_\tau^2}\langle uv\rangle\frac{\partial\tilde{u}}{\partial\eta}-\frac{\langle\varepsilon_1\rangle}{\omega u_\tau^2} \tag{9}$$

$$\tilde{F}=\frac{\partial\tilde{U}_e}{\partial\tilde{t}}+\tilde{U}_e\frac{\partial\tilde{U}_e}{\partial\tilde{x}} \tag{10}$$

The scaling length $b(x)$ is prescribed appropriate to the specific flow situation. For example, $b=$ constant corresponds to the use of physical cross-stream distances and is suitable for bounded flows such as flow in a channel or between two parallel plates. For the solution of periodic laminar boundary layer flows, b can be made equal to either the Blasius boundary layer thickness $\sqrt{(\nu x/U_0)}$ (or, better still, the boundary layer thickness in steady flow with the same time-mean pressure gradient) or to the so called Stokes layer thickness $(\nu/\omega)^{1/2}$, depending on the oscillation frequency. Likewise, for periodic turbulent flows an appropriate turbulent boundary layer thickness can be used for b.

2.3. *Discretization*

The non-dimensional unsteady boundary layer equations are discretized using an adaptation of the implicit finite difference scheme proposed by Oskolkov.[16] To illustrate the procedure, the discretized versions of the momentum and continuity equations for *laminar*

flow, i.e. equations (8) and (7) with $\langle uv \rangle = 0$, are shown below, with $b(x) = \sqrt{(\nu x/U_0)}$,

$$\frac{\tilde{u}_{ij}^{l+1} - \tilde{u}_{ij}^{l}}{\Delta \tilde{t}} + \tilde{u}_{ij}^{l} \frac{(\tilde{u}_{ij}^{l+1} - \tilde{u}_{i-1\,j}^{l+1})}{\Delta \tilde{x}} - \frac{\tilde{u}_{ij}^{l} \eta_j}{2\tilde{x}_i} \frac{(\tilde{u}_{ij}^{l+1} - \tilde{u}_{ij-1}^{l+1})}{\Delta \eta_{jj-1}} + \tilde{v}_{ij}^{l} \frac{(\tilde{u}_{ij}^{l+1} - \tilde{u}_{ij-1}^{l+1})}{\Delta \eta_{jj-1}} \tag{11}$$

$$= \frac{2}{\tilde{x}_i (\Delta \eta_{j+1\,j} + \Delta \eta_{jj-1})} \left(\frac{\tilde{u}_{i\,j+1}^{l+1} - \tilde{u}_{ij}^{l+1}}{\Delta \eta_{j+1\,j}} - \frac{\tilde{u}_{ij}^{l+1} - \tilde{u}_{ij-1}^{l+1}}{\Delta \eta_{jj-1}} \right) + \tilde{F}_{ij}^{l+1}$$

$$\frac{\tilde{u}_{ij}^{l+1} - \tilde{u}_{i-1\,j}^{l+1}}{\Delta \tilde{x}} - \frac{\eta_j}{2\tilde{x}_i} \frac{(\tilde{u}_{ij}^{l+1} - \tilde{u}_{ij-1}^{l+1})}{\Delta \eta_{jj-1}} + \frac{\tilde{v}_{ij}^{l+1} - \tilde{v}_{ij-1}^{l+1}}{\Delta \eta_{jj-1}} = 0 \tag{12}$$

where i, j and l are the indices in the $\tilde{x}$, η and $\tilde{t}$ directions, respectively, and $i = 1, 2, \ldots I$; $j = 1, 2, \ldots J$; $l = 1, 2, \ldots$. Equations (11), with $j = 1, 2, \ldots J$, are solved simultaneously for each column i. The solution is obtained by means of the efficient tridiagonal algorithm. Once $\tilde{u}_{ij}^{l+1}$ is known from $j = 1$ to J, $\tilde{v}_{ij}^{l+1}$ is calculated according to equation (12).

Note that the convection terms in the momentum equation have been linearized in their discrete version, equation (11). It was found that for oscillatory flow this is accurate enough.

2.4. *Initial and upstream boundary conditions*

In the case of periodic flows, the steady state solution corresponding to the time-average of $U_e(x, t)$ is used (for convenience) as the initial condition for the calculation. This solution can be obtained by starting with an arbitrary state and using the same numerical scheme as a relaxation procedure with the free-stream velocity constant in time at its time-mean value, till convergence is obtained. Calculation of the unsteady flow is then continued by prescribing the required free-stream condition for $\tilde{F}$, namely equation (10). The final periodic state is reached after the initial transient dies out.

The appropriate upstream boundary conditions must be supplied from experimental information. In the absence of experimental information, specification of upstream boundary conditions poses one of the major problems, particularly if the unsteady effects are completely unknown in advance. In such cases, one has to assume some reasonable upstream boundary condition and hope that the uncertainty in the predictions will eventually die out at far-downstream locations. The quasi-steady solution (i.e. the solution corresponding to a periodic flow at an infinitely low frequency of oscillation) has been employed as the upstream boundary condition in most of the calculations reported here. This assumption, however, needs to be tested in each particular problem.

2.5. *Preliminary test problems*

The numerical method in its general (non-periodic) form was first tested by applying it to various simple laminar shear flow problems for which exact solutions are known. These included a steady flow (the flat plate boundary layer), an unsteady non-periodic flow (the evolution of Couette flow) and an unsteady but periodic flow (fully developed periodic flow in a two-dimensional channel). In all the cases the results were quite satisfactory. These tests and results are described in detail by Menendez and Ramaprian.[17]

3. CALCULATION OF PERIODIC LAMINAR BOUNDARY LAYERS WITH SMALL AMPLITUDES OF OSCILLATION

3.1. *Introduction*

The method of calculation will now be applied to solve Blasius and Howarth mean flows subjected to oscillations of small amplitude in the free-stream velocity. These flows have

been chosen, since asymptotic analytical solutions, as well as experimental data, are available. It is well established for these problems that the extent of unsteady effects varies with the frequency of oscillation. For low frequencies, they manifest all across the thickness of the boundary layer. For high frequencies, in turn, the unsteady effects are confined to a layer of smaller thickness close to the wall, namely the Stokes layer. The mathematical criterion to distinguish between low and high frequencies is

$$\tilde{x} \ll 1\text{: low frequencies}$$

$$\tilde{x} \gg 1\text{: high frequencies}$$

In fact, $\tilde{x}$ can be written as $\tilde{x} = [\sqrt{(\nu x/U_0)}/\sqrt{(\nu/\omega)}]^2$, and is thus a measure of the ratio of the Blasius to the Stokes layer thickness.

3.2. *Blasius mean flow*

For a free-stream velocity given by

$$U_e(x, t) = \bar{U}_e(1 + \varepsilon \sin \omega t) \tag{13}$$

with $\bar{U}_e = U_0 =$ constant and $\varepsilon \ll 1$, the velocity profile can be approximated, to first order, by

$$U(x, y, t) = U_B(x, y) + \varepsilon \Delta u(x, y) \sin [\omega t + \phi(x, y)] \tag{14}$$

where U_B is the Blasius velocity distribution, and the second term represents the periodic perturbation. The calculations were performed with the following set of data:

$$Re_{x_0} = \frac{U_0 x_0}{\nu} = 10{,}000, \qquad \varepsilon \sim 0{\cdot}10, \qquad N = 100, \qquad I = 31, \qquad J = 100 \tag{15}$$

For any given value of $\tilde{x}$, the values of $\tilde{x}_0$ and $\Delta\tilde{x}$ are calculated such that the upstream and downstream stations are separated by a distance of 100 boundary layer thicknesses at $\tilde{x}_0$. The value of Re_{x_0} is used only for estimating the boundary layer thickness at $\tilde{x}_0$.

Figure 1 shows the calculated and theoretical mean velocity profiles for $\tilde{x} = 1{\cdot}48$. For small amplitudes, the theoretical profile is simply the steady Blasius solution. Good agreement is observed between theory and numerical calculations. The result is typical for the range of $\tilde{x}$ values analysed.

Figures 2(a) and (2b) present results for the relative amplitude of oscillation $\Delta u/U_0$ and the phase of the oscillation ϕ relative to the free stream, in the low frequency range $\tilde{x} < 0{\cdot}6$. Also shown there is the low frequency ($\omega \to 0$) solution by Lighthill,[3] and some points from the experiments of Hill and Stenning.[5] Even for the lowest value of $\tilde{x}$ shown (0·103), the theoretical asymptotic solution shows some deviation from the calculated one. When $\tilde{x}$ increases, the deviation increases. This is to be expected, since the Lighthill solution gradually breaks down with the increase in frequency. In general, though, the calculated results are in better agreement with the measurements of Hill and Stenning.[5]

For $\tilde{x} > 0{\cdot}6$, generally regarded as the high frequency range, the results are shown in Figures 3(a) and (3b). They are presented in terms of the Stokes coordinate $\eta_s = y\sqrt{(\omega/2\nu)}$, and compared with the Lighthill high frequency solution,[3] which is essentially the shear wave solution, namely

$$\tilde{U}_{osc} = (U - U_B)/\varepsilon U_0 = \cos \tilde{t} - \exp(-\eta_s) \cos(\tilde{t} - \eta_s) \tag{16}$$

Points corresponding to the experiments of Hill and Stenning[5] are also shown, together with

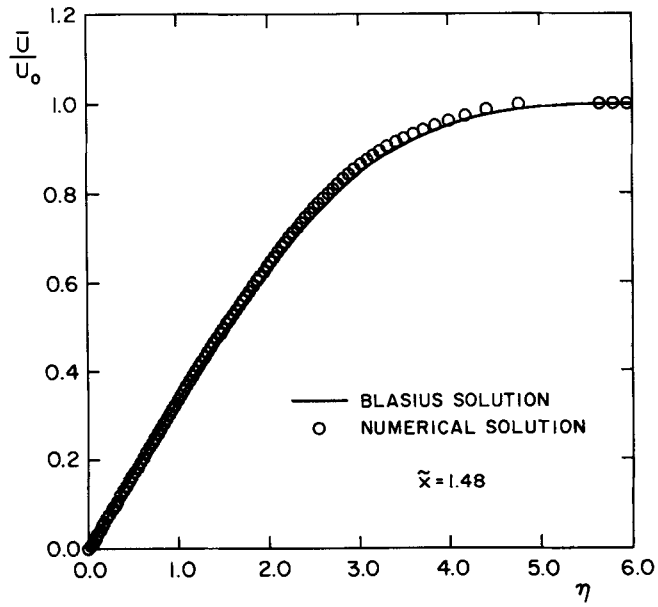

Figure 1. Periodic laminar boundary layer at zero-mean pressure gradient: time-mean velocity profile

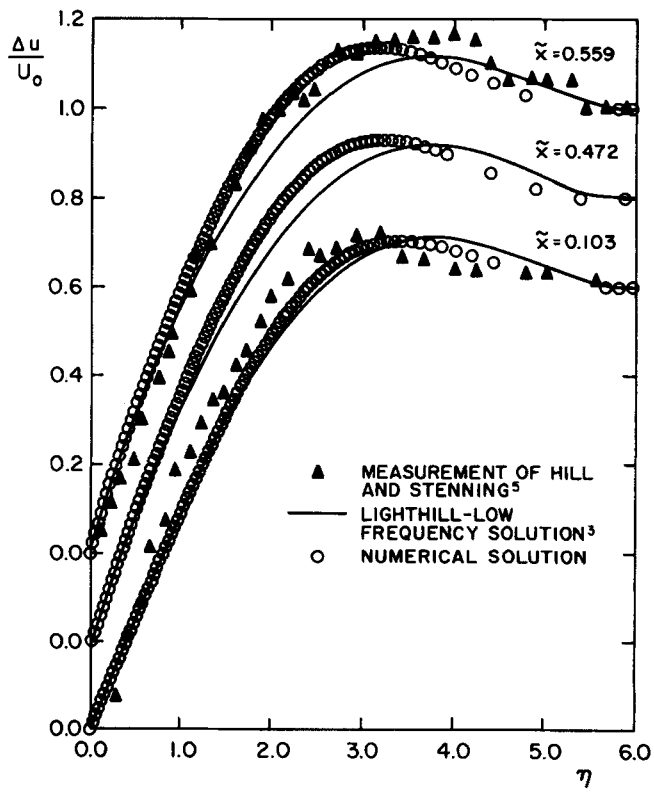

Figure 2(a). Periodic laminar boundary layer at zero-mean pressure gradient: amplitude of oscillation for low frequencies

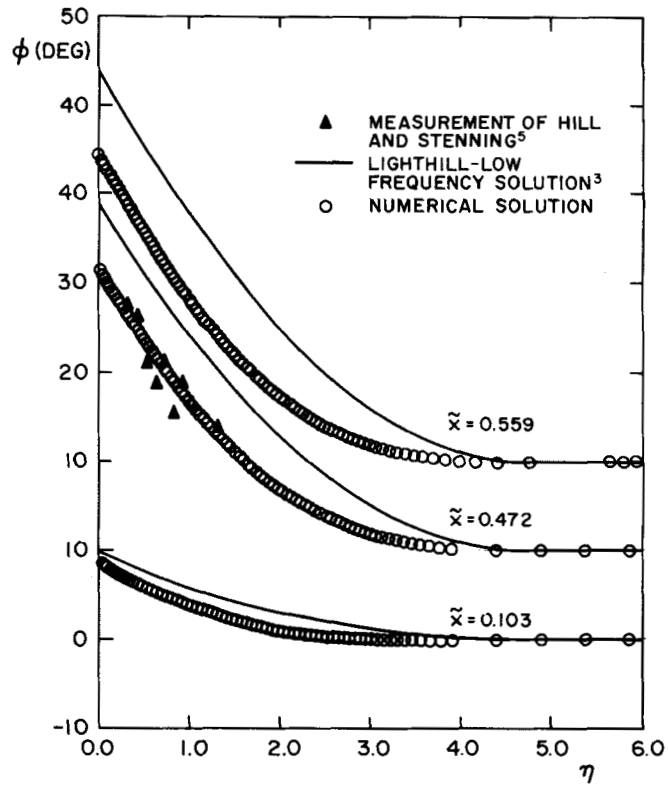

Figure 2(b). Periodic laminar boundary layer at zero-mean pressure gradient: phase of oscillation for low frequencies

their theoretical solution. They developed a calculation for intermediate and high frequencies based on the shear wave solution, but taking first order convective effects into account. The present numerical calculations and the calculations of Hill and Stenning agree reasonably well with each other and with the experimental results, and all these approach the shear wave solution for large values of $\tilde{x}$ ($\tilde{x} = 4{\cdot}98$).

Within the adopted methodology more grid points in the $\tilde{x}$-direction should be necessary in order to carry the computations to even larger values of $\tilde{x}$ than discussed above. This is in order to ensure independence of results from upstream boundary conditions, taken as the quasi-steady solution. The disadvantage of this procedure is that computer time increases significantly, making the calculation uneconomical. The natural alternative seems to maintain the original number of nodes, but impose a more realistic upstream boundary condition. The best choice is the shear wave solution. Calculations were made for $\tilde{x} = 20$ using this procedure. The results for the amplitude and phase, shown in Figures 3(a) and 3(b), respectively, are satisfactory.

3.3. *Howarth mean flow*

For a free-stream velocity given by

$$U_e(x, t) = U_0(1 - \hat{x} + \varepsilon \sin \omega t) \tag{17}$$

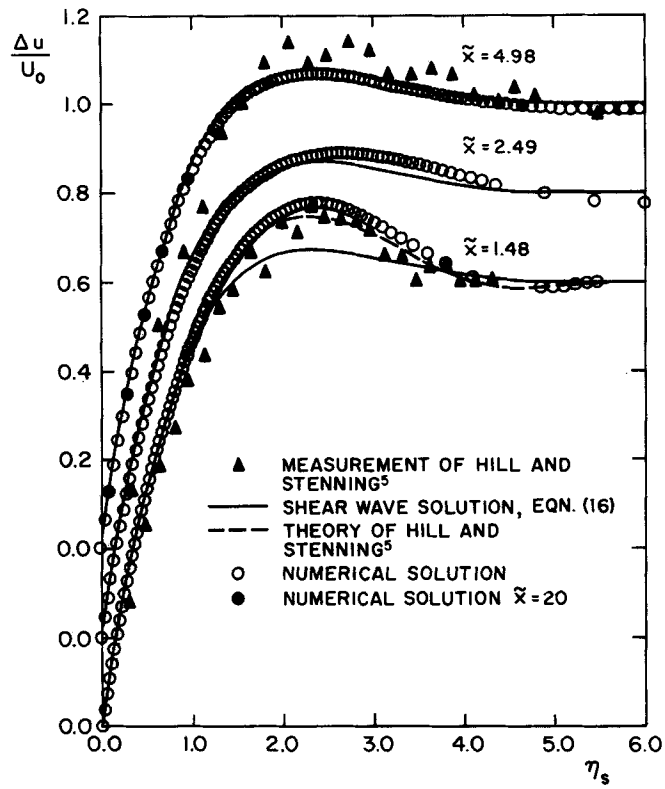

Figure 3(a). Periodic laminar boundary layer at zero-mean pressure gradient: amplitude of oscillation for high frequencies

where $\varepsilon \ll 1$ and $\hat{x} \equiv b_1 x/U_0$, with $b_1 =$ constant, the velocity profile depends on two parameters, namely $\tilde{x}$ and $\hat{x}$. However, all the calculations were performed for $\hat{x} = 0{\cdot}1$ (close to $\hat{x} = 0{\cdot}12$, the location of the separation point in steady Howarth flow[18]) to compare with the theoretical and experimental results of Hill and Stenning. The following data were used:

$$Re_{x_0} = 10{,}000, \qquad \hat{x} = 0{\cdot}1, \qquad \varepsilon \sim 0{\cdot}1, \qquad N = 100, \qquad I = 31, \qquad J = 100 \qquad (18)$$

The distance between $\tilde{x}_0$ and $\tilde{x}$ was varied from 100 boundary layer thicknesses (mean value at $\tilde{x}_0$) for the lower frequencies to 300 boundary layer widths for the higher ones. This was necessary in order to avoid the effects of the upstream boundary condition. It was also found that flow reversal (but not separation) occurred near the wall for some of the cases studied. A modification of the numerical scheme was found to be necessary in order to handle such reverse flow regions. This modification is described in Section 3.5.

Figure 4 shows the calculated time-mean velocity profile for $\tilde{x} = 2{\cdot}31$, together with the theoretical profile which, for small amplitudes, is identical to that for steady Howarth flow. The agreement is quite good, and is typical for all the range of $\tilde{x}$ analysed.

Figures 5(a) and 5(b) present the results for the amplitude and phase of the oscillation in the low frequency range. The Lighthill low frequency asymptotic solution, as evaluated by Hill and Stenning,[5] is also shown together with experimental data from the same authors. The agreement between calculation and measurements is less satisfactory now than in the previous case. The Lighthill solution, on the other hand, is not accurate, in principle, at these

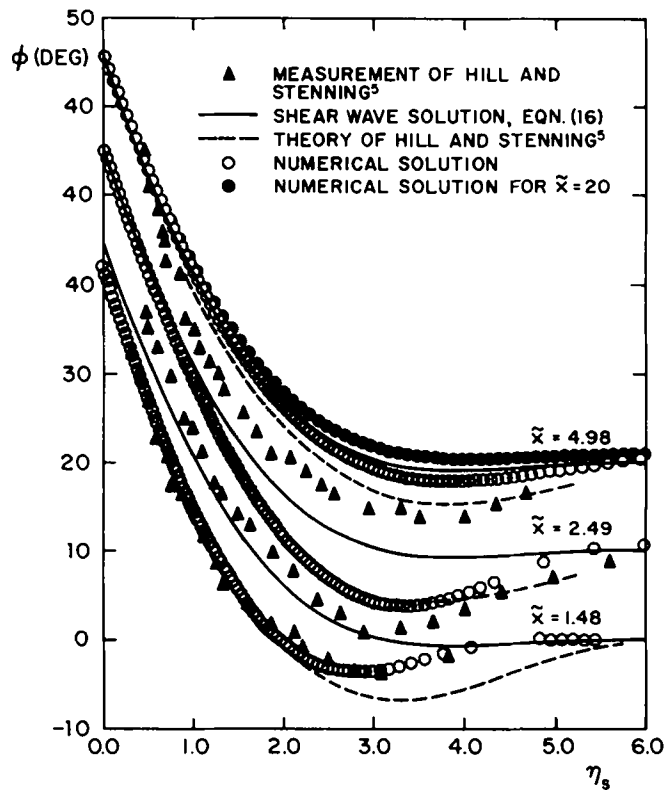

Figure 3(b). Periodic laminar boundary layer at zero-mean pressure gradient: phase of oscillation for high frequencies

values of $\tilde{x}$. Its agreement with the experimental results for the phase when $\tilde{x} = 0{\cdot}450$ must then be considered accidental. It must also be recognized that phase measurements at these low frequencies could be quite inaccurate.

Results for the intermediate and high frequency range are shown in Figures 6(a) and 6(b). They are compared with the Lighthill high frequency solution [again the shear wave solution, equation (16)] and with the Hill and Stenning theoretical and experimental results.[5] The results are shown using the Stokes coordinate η_s as the cross-stream variable. The theory of Hill and Stenning give results which agree reasonably well with the calculation. The discrepancy between calculation and measurements, in turn, could perhaps be due to the difficulties encountered in simulating and measuring a periodic flow of this type.

For both Blasius and Howarth mean flow problems, complete stabilization of the periodic numerical solution was achieved just after one cycle for small $\tilde{x}$, and after two cycles for large $\tilde{x}$. Computer time was about 0·018 s per time step and per column (of 100 points) on an IBM 370/168.

3.4. *Step sizes*

The time step used throughout the calculations presented in the last two sections was $\Delta\bar{t} = 0{\cdot}0628$, corresponding to a total number of time steps, $N = 100$. The grid size in the η-direction is not constant. The grid point locations were adjusted so as to give a uniform

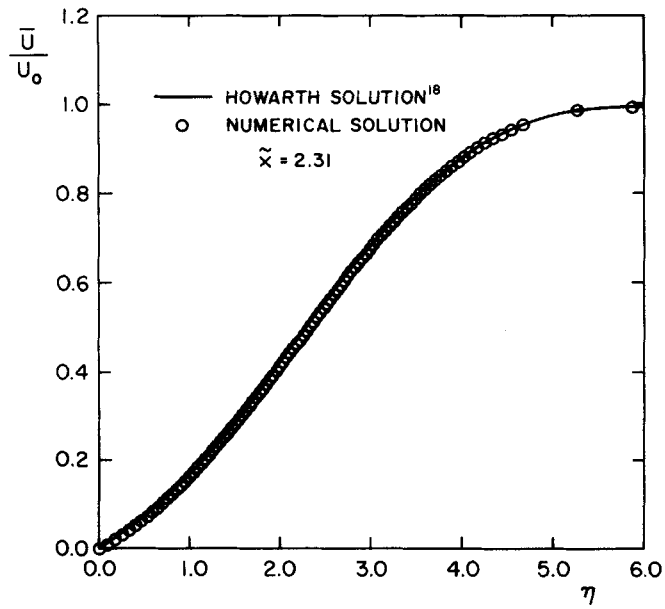

Figure 4. Periodic laminar boundary layer for Howarth mean flow: time-mean velocity profile

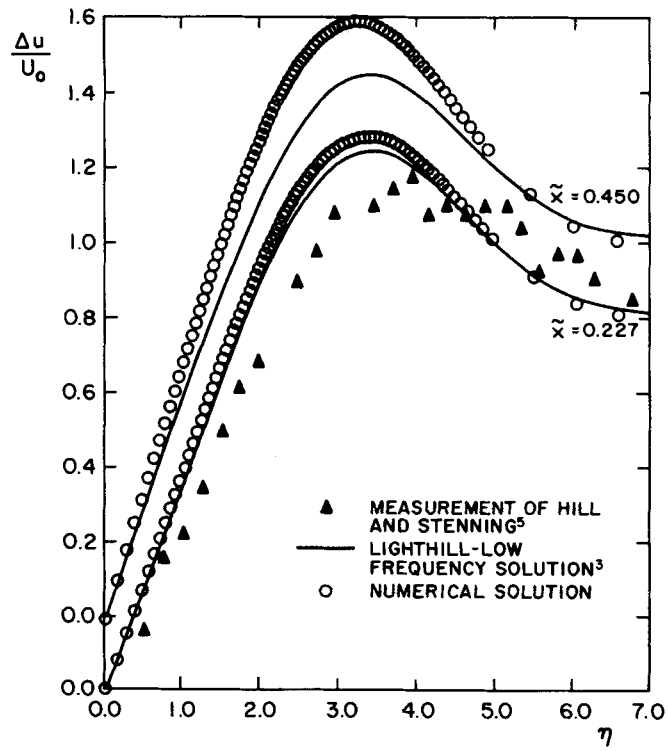

Figure 5(a). Periodic laminar boundary layer for Howarth mean flow: amplitude of oscillation for low frequencies

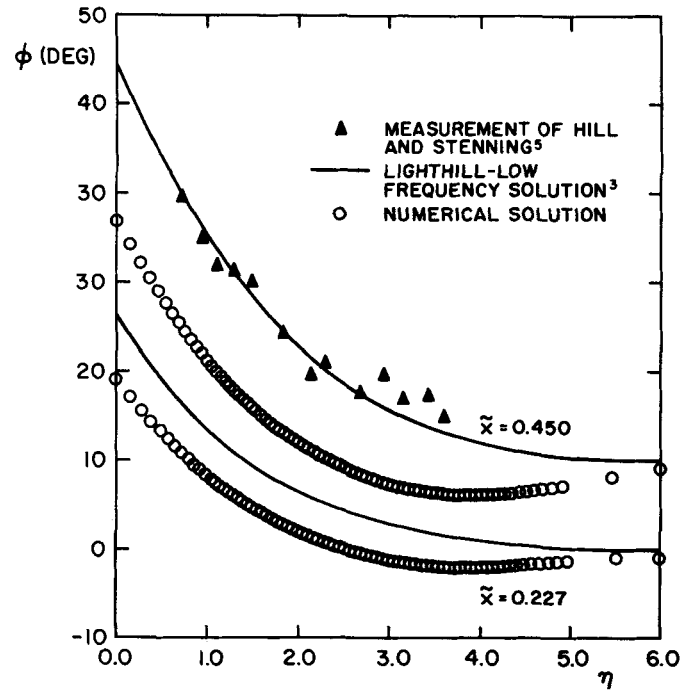

Figure 5(b). Periodic laminar boundary layer for Howarth mean flow: phase of oscillation for low frequencies

velocity increment across the boundary layer (except for a few points at the outer edge, to avoid too low a density of points there). Typically, $\Delta\eta$ varied from 0·05 near the wall to 0·65 at the outer edge, for $J = 100$. The grid size in the $\tilde{x}$-direction was maintained constant in a given run. It was calculated for each run, by fixing the distance between $\tilde{x}_0$ and $\tilde{x}$ (100–300 boundary layer thicknesses) and the number of grid points $I(=31)$ between them. In this way $\Delta\tilde{x}$ typically ranged from 0·003 (for small $\tilde{x}$) to 0·14 (for large $\tilde{x}$). The sensitivity of the numerical solution to variations in the step sizes was appropriately checked, and the above values were found to be satisfactory.[17]

3.5. *Handling of flow reversal*

The upwind differencing of convective terms in equation (11) becomes inaccurate (and eventually unstable) when one or both of the velocity components are negative. In fact, for mean adverse pressure gradient flows (such as Howarth flow), for large amplitudes of oscillation, or for high frequencies of oscillation, flow reversal is likely to occur during part of the cycle. This does not (necessarily) mean separation, in the sense of breakdown of the boundary layer approximation. For regions of the flow in which such flow reversal (but not separation) occurs, the convective terms in equation (11) are discretized according to

$$\left[\tilde{u}\frac{\partial\tilde{u}}{\partial\tilde{x}}\right]_{ij} = \begin{cases} \tilde{u}_{ij}^{l}\dfrac{(\tilde{u}_{ij}^{l+1} - \tilde{u}_{i-1j}^{l+1})}{\Delta\tilde{x}} & \text{for} \quad \tilde{u}_{ij}^{l} > 0 \\ \tilde{u}_{ij}^{l}\dfrac{(\tilde{u}_{i+1j}^{l} - \tilde{u}_{ij}^{l+1})}{\Delta\tilde{x}} & \text{for} \quad \tilde{u}_{ij}^{l} < 0 \end{cases} \tag{19}$$

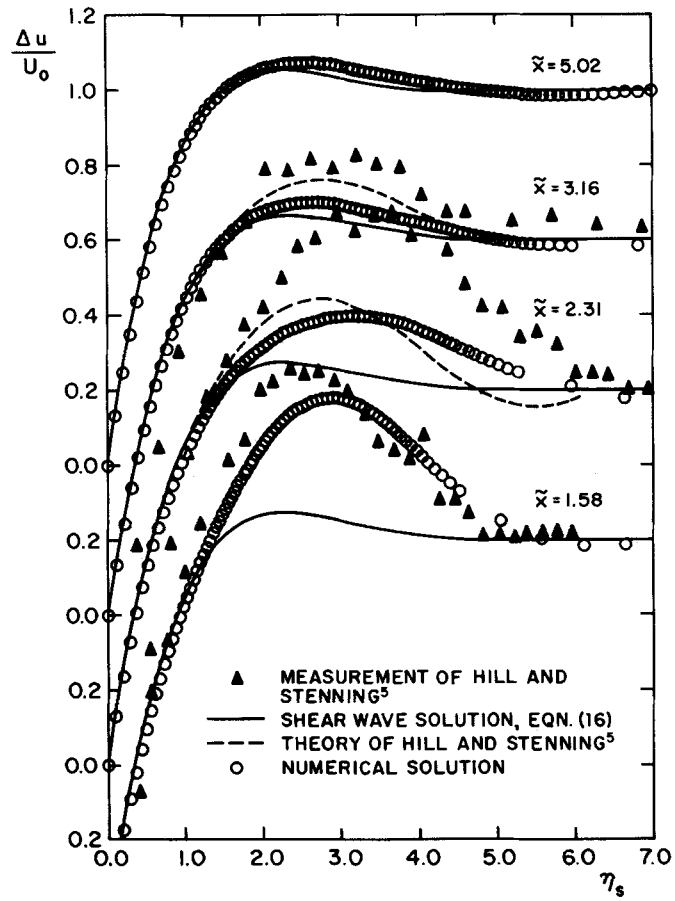

Figure 6(a). Periodic laminar boundary layer for Howarth mean flow: amplitude of oscillation for high frequencies

$$\left[\tilde{v}\frac{\partial\tilde{u}}{\partial\eta}\right]_{ij} = \begin{cases} \tilde{v}_{ij}^{l}\dfrac{(\tilde{u}_{ij}^{l+1}-\tilde{u}_{ij-1}^{l+1})}{\Delta\eta_{jj-1}} & \text{for} \quad \tilde{v}_{ij}^{l}>0 \\ \tilde{v}_{ij}^{l}\dfrac{(\tilde{u}_{ij+1}^{l+1}-\tilde{u}_{ij}^{l+1})}{\Delta\eta_{j+1j}} & \text{for} \quad \tilde{v}_{ij}^{l}<0 \end{cases} \tag{20}$$

The term $-(\eta/2\tilde{x})\tilde{u}\,\partial\tilde{u}/\partial\eta$ in equation (11) was left unchanged, as the quantity being convected is a derivative in a normal direction relative to the velocity. It is seen that for the case $\tilde{u}_{ij}^{l}<0$, $\tilde{u}_{i+1j}^{l}$ is not known at the last downstream station. For this station, therefore, the value at the previous time level, namely $\tilde{u}_{ij}^{l}$, is used instead. To avoid a direct impact of this procedure on the velocity profiles at a given $\tilde{x}$, five additional grid-points are used beyond this station (increasing I from 31 to 36).

The results obtained with this numerical scheme for the Howarth-mean-flow problem discussed in Section 3.3, were found to be satisfactory. These results were further checked by performing analogous calculations for much smaller absolute amplitudes of oscillation ($\varepsilon = 0{\cdot}01$) for which no flow reversal occurs.[17]

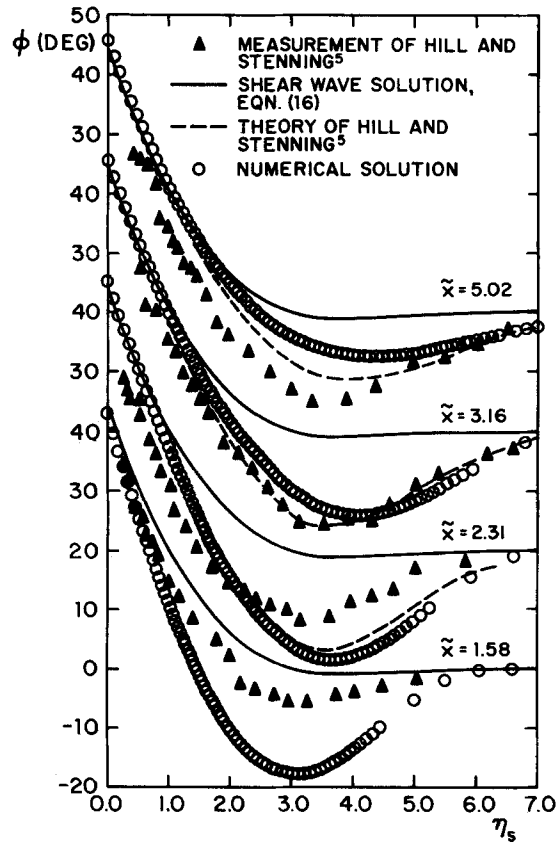

Figure 6(b). Periodic laminar boundary layer for Howarth mean flow: phase of oscillation for high frequencies

4. PERIODIC LAMINAR BOUNDARY LAYERS AT LARGE AMPLITUDES OF OSCILLATION

The case of periodic boundary layers with large oscillation amplitude deserves a separate study. In fact, for a free-stream velocity given by equation (13) with arbitrary ε, the velocity profile depends now on the two parameters $\tilde{x}$ and ε. Then, the asymptotic solutions referred to in the previous section will not be applicable except at high frequencies ($\omega \to \infty$). As far as the authors are aware, the only solution available for such flows is that obtained by Pedley[7] using both regular (for $\omega \to 0$) and singular (for $\omega \to \infty$) asymptotic expansions. Even these are essentially numerical solutions and are available for the skin friction and surface heat transfer only. No experimental data are available at present.

Calculations for $\varepsilon = 0{\cdot}5$ were performed for various values of $\tilde{x}$. The remaining data were the same as those in equation (15), and the distance between $\tilde{x}$ and $\tilde{x}_0$ was taken as 100 boundary layer thicknesses.

Figures 7(a) and 7(b) show the calculated evolution of the wall shear stress with time during the oscillation cycle for $\tilde{x} = 0{\cdot}1$, $0{\cdot}6$ and 4. The theoretical solution of Pedley[7] for the same amplitude, $\varepsilon = 0{\cdot}5$, is also presented. Good agreement is observed for the two extreme cases, $\tilde{x} = 0{\cdot}1$ and $\tilde{x} = 4$. In the first case, the comparison is made with the asymptotic

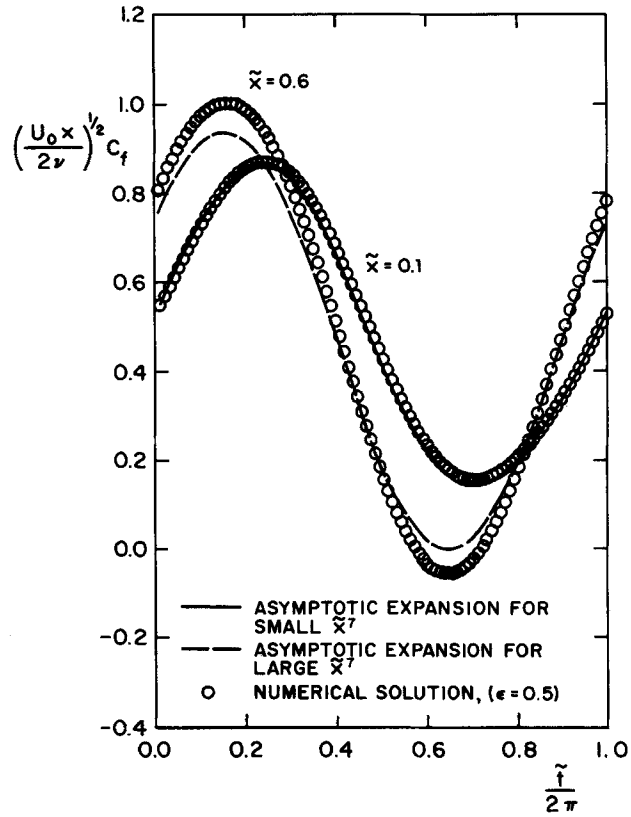

Figure 7(a). Skin friction at large amplitude for low and intermediate frequency

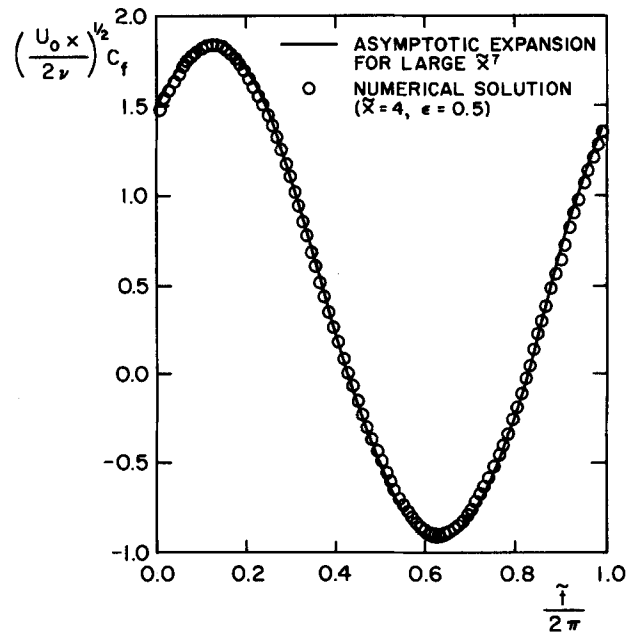

Figure 7(b). Skin friction at large amplitude for high frequency

expansion for small $\tilde{x}$. In the second case, the asymptotic expansion for large $\tilde{x}$ is used. The intermediate case, $\tilde{x}=0{\cdot}6$, corresponds to the overlapping zone, and hence some departure can be expected. Negative values of the wall shear stress in Figures 7(a) and 7(b) indicate the existence of a backflow region. It is seen that the numerical scheme works satisfactorily even with strong flow reversals (large negative wall shear stress).

5. PERIODIC TURBULENT BOUNDARY LAYERS

After performing the rigorous tests described in the previous sections to establish the accuracy of the numerical procedure for laminar flow, the method was extended to calculate periodic turbulent boundary layers, using well-known and simple turbulence closure models. These are the Prandtl mixing length model (a zero-equation model) and the Prandtl energy (k–L) model (a one-equation model). A recent experiment by Parikh, Reynolds and Jayaraman[21] has been used as the test case.

The details of the two models are given below.

(a) Mixing length model: The Reynolds stress $\langle uv\rangle$ in equation (2) is expressed as[12,17]

$$\langle uv\rangle = -\langle l_m\rangle^2 \left|\frac{\partial\langle U\rangle}{\partial y}\right| \frac{\partial\langle U\rangle}{\partial y} \tag{21}$$

where $\langle l_m\rangle$ is the mixing length, prescribed by

$$\langle l_m\rangle = 0{\cdot}095\langle\delta\rangle \tanh\{0{\cdot}4y[1-\exp(-y\langle U_\tau\rangle/26\nu)]/(0{\cdot}095\langle\delta\rangle)\} \tag{22}$$

In this case, only equations (1) and (2) are solved.

(b) k–L model: The assumptions are[17,19,20]

$$\langle uv\rangle = -C_1\sqrt{(2\langle k\rangle)}\langle l_k\rangle\left[1-\exp\left(-\frac{C_3\sqrt{(2\langle k\rangle)}y}{\nu}\right)\right]\frac{\partial\langle U\rangle}{\partial y} \tag{23}$$

$$\langle(q^2/2+p/\rho)v\rangle = -C_2\sqrt{(2\langle k\rangle)}\langle l_k\rangle\left[1-\exp\left(-\frac{C_3\sqrt{(2\langle k\rangle)}y}{\nu}\right)\right]\frac{\partial\langle k\rangle}{\partial y} \tag{24}$$

$$\langle\varepsilon_1\rangle = C_4\frac{(2\langle k\rangle)^{3/2}}{\langle l_k\rangle}\left(1+\frac{C_5\nu}{\sqrt{(2\langle k\rangle)}\langle l_k\rangle}\right) \tag{25}$$

with the length scale $\langle l_k\rangle$ being defined as

$$\frac{\langle l_k\rangle}{\langle\delta\rangle} = \begin{cases} 0{\cdot}095\tanh\left(\dfrac{0{\cdot}4y}{0{\cdot}095\langle\delta\rangle}\right) & \text{for } \dfrac{y}{\langle\delta\rangle}\le 0{\cdot}5 \\ 0{\cdot}095-0{\cdot}055\left(2\dfrac{y}{\langle\delta\rangle}-1\right)^2 & \text{for } 0{\cdot}5<\dfrac{y}{\langle\delta\rangle}\le 1{\cdot}1 \\ 0{\cdot}0158\exp\left[-10\left(\dfrac{y}{\langle\delta\rangle}-1{\cdot}1\right)\right] & \text{for } \dfrac{y}{\langle\delta\rangle}>1{\cdot}1 \end{cases} \tag{26}$$

The empirical constants are given their usual values, which are

$$C_1 = C_2 = 0{\cdot}39, \qquad C_3 = 0{\cdot}0136, \qquad C_4 = 0{\cdot}0593, \qquad C_5 = 2{\cdot}698 \tag{27}$$

Now, the three equations, (1)–(3), are used.

Both turbulence models are used in a quasi-steady form, by relating the ensemble averaged shear stress $\langle uv\rangle$ to the ensemble averaged flow properties at the same phase

position. Also in both cases the finite difference calculations are carried up to the wall without the use of any algebraic wall functions.[22] Such functions are not known *a priori* for unsteady turbulent flows. In order to ensure that the numerical procedure works correctly for turbulent flows, calculations were first made for steady turbulent boundary layer in zero-pressure gradient, with good results.[17]

In the experiments of Parikh, Reynolds and Jayaraman,[21] the free-stream velocity distribution is given by

$$U_e(x,t)=\begin{cases} U_0 & \text{for } x<x_0 \\ U_0-\dfrac{a_0(x-x_0)}{L_0}(1-\cos 2\pi ft) & \text{for } x_0\leq x<x_0+L_0 \end{cases} \tag{28}$$

Thus, there exists a steady zero-pressure gradient for $x<x_0$ and a periodic adverse pressure gradient from $x=x_0$ to $x=L_0$. The values of the various flow parameters are:

$$\begin{gathered} U_0=0{\cdot}73\text{ m/s}, \quad x_0=2\text{ m}, \quad L_0=0{\cdot}6\text{ m}, \quad \delta_0=0{\cdot}05\text{ m}, \quad a_0=0{\cdot}05U_0 \\ f=0{\cdot}0\text{ Hz}, \quad 0{\cdot}25\text{ Hz}, \quad 0{\cdot}5\text{ Hz} \quad \text{and} \quad 2{\cdot}0\text{ Hz} \end{gathered} \tag{29}$$

Calculations were performed for frequencies of 0·01 Hz, 0·25 Hz, 0·5 Hz, and 2·0 Hz. The first frequency can be regarded as nearly quasi-steady. In all these calculations the upstream boundary conditions for $\langle U\rangle(x_0, y, t)$ and $\langle k\rangle(x_0, y, t)$ corresponded to a standard steady zero-pressure gradient turbulent boundary layer, and the initial conditions were taken as the steady state at the time-mean pressure gradient. Equations (7)–(10) were used with the scaling length $b(x)$ and velocity $u_\tau(x)$ being chosen as

$$b(x)=0{\cdot}14\frac{\nu}{U_0}Re_x^{6/7} \tag{30}$$

$$u_\tau(x)=\sqrt{0{\cdot}013U_0Re_x^{-1/14}} \tag{31}$$

The above expressions are correlation formulae proposed by White[23] for the boundary layer thickness and the shear velocity, respectively, along a flat plate, with $Re_x = U_0x/\nu$. A total of 101 grid points were used in the cross-stream direction. These were variably spaced so as to give equal velocity intervals at the downstream station. A total of 30 steps were used in the $\tilde{x}$-direction and 100 time steps per cycle. Some typical results of the above calculations are shown and compared with experiments in Figures 8, 9(a) and 9(b). Comparisons are also shown with similar calculations made by Orlandi[13] using a nearly identical k–L model but a different numerical scheme. More results and comparisons can be found in Reference 17.

In the experiments, the time-mean velocity distribution across the boundary layer was found to be unaffected by the imposed oscillation and equal to that in steady flow under the time-mean pressure gradient conditions. The calculation indicated practically the same (Figure 8). It is seen that the k–L model gives a slightly better prediction.

Figures 9(a) and 9(b) show the results for the amplitude, ΔU and phase, ϕ of the periodic velocity, respectively, when $f=0{\cdot}25$ Hz (in these Figures, $\Delta U_e = a_0(x-x_0)/L_0$). The prediction of the amplitude is satisfactory in an overall sense though the two-models deviate from the experimental results in detail. Also shown in Figure 9(a) is the numerical solution of Orlandi. He used the same modelling assumptions, equations (23)–(25), though equation (24) was used to model only the kinetic energy diffusion part. The pressure-strain term was modelled separately. He also employed a different (but essentially equivalent) analytical expression for the length scale $\langle l_k\rangle$ and used slightly different values for the empirical

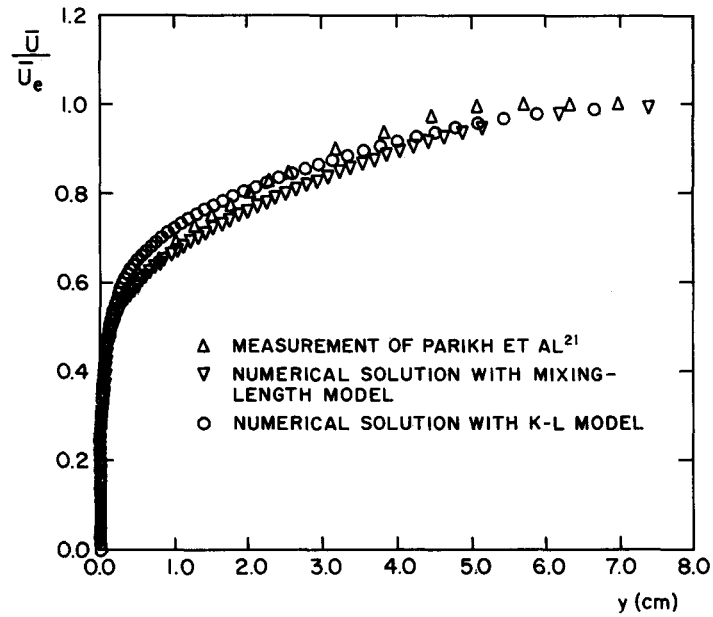

Figure 8. Periodic turbulent boundary layer in adverse pressure gradient: time-mean velocity profile

constants. His calculation underpredicts the amplitude. In fact, the same was found to be true for the quasi-steady case.[17] However, this discrepancy between the present calculations and those of Orlandi appeared to decrease with increasing frequency. The prediction of the phase by both the turbulence models studied seems to be in general agreement with the experiment and can be considered to be satisfactory in view of the experimental uncertainties and the simplicity of the models used.

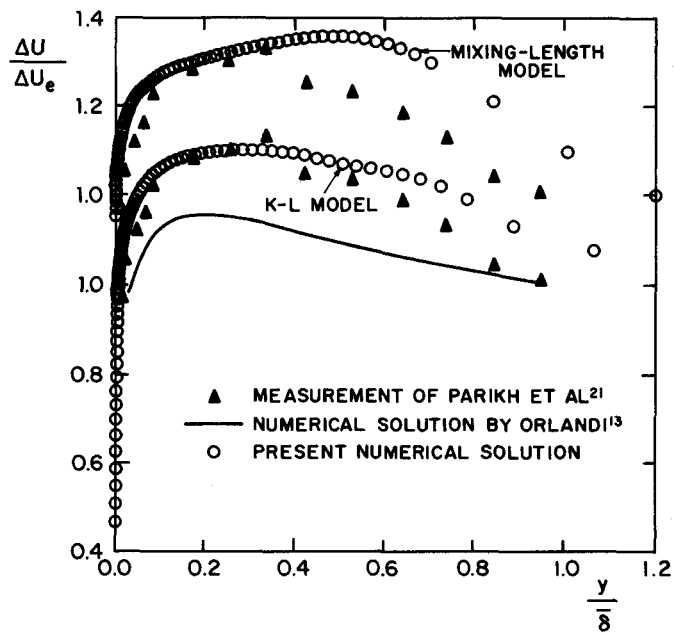

Figure 9(a). Periodic turbulent boundary layer in adverse pressure gradient: amplitude of oscillation for $f = 0{\cdot}25$ Hz

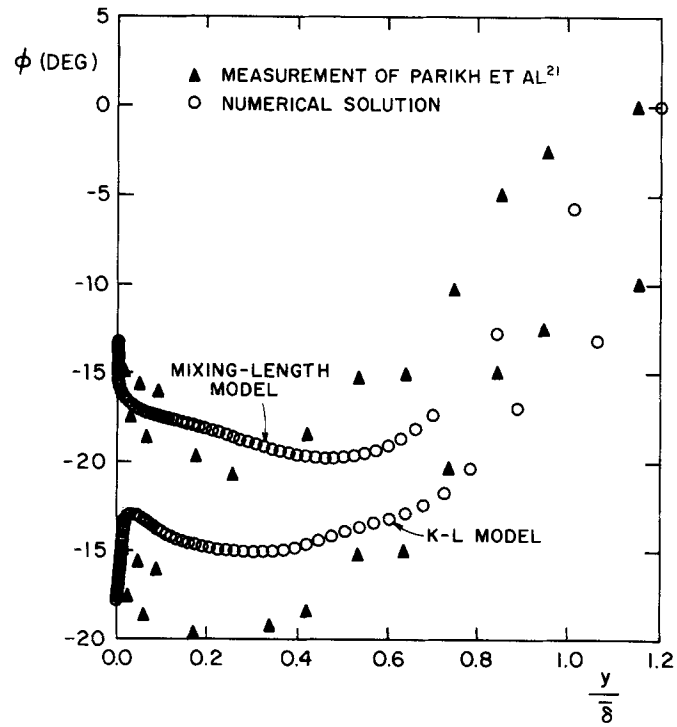

Figure 9(b). Periodic turbulent boundary layer in adverse pressure gradient: phase of oscillation for $f = 0{\cdot}25$ Hz

6. CONCLUSIONS

An implicit, finite difference procedure for the prediction of time-dependent boundary layer flows has been developed. The method has been demonstrated to be accurate at small and large frequencies, at all amplitudes and even when there is flow reversal during a part of the cycle in a periodic laminar flow. When applied to a simple turbulent flow, its predictions show good agreement with the available experimental results.

ACKNOWLEDGEMENTS

The study reported here was supported by the U.S. Army Research Office through Grants No. DAAG29-79-G-0017 and DAAG29-83-K-0004, with Dr. R. E. Singleton as Scientific Program Officer. The authors gratefully acknowledge this support.

NOTATION

b = transverse length scale
C_f = local skin friction coefficient, $\tau_w/(\frac{1}{2}\rho\bar{U}_e^2)$
f = frequency of oscillation
k = instantaneous turbulent kinetic energy
$\bar{k}$ = $\langle k \rangle / u_\tau^2$ = dimensionless turbulent kinetic energy
N = number of time steps per cycle

p = instantaneous pressure
q = $[2k]^{1/2}$
t = time co-ordinate
$\tilde{t}$ = ωt = dimensionless time
U = instantaneous streamwise velocity component
U_0 = streamwise velocity scale
U_τ = shear velocity
u = turbulent fluctuation of U
u_τ = velocity scale for the turbulence
$\tilde{u}$ = $\langle U \rangle / U_0$ = dimensionless streamwise velocity component
V = instantaneous cross-stream velocity component
v = turbulent fluctuation of V
$\tilde{v}$ = $\langle V \rangle / \omega b$ = dimensionless cross-stream velocity component
x = streamwise co-ordinate
$\tilde{x}$ = $\omega x / U_0$ = dimensionless streamwise co-ordinate
y = cross-stream co-ordinate
$\Delta\tilde{t}$ = time step size
ΔU = amplitude of the periodic component of U
Δu = $\Delta U / \varepsilon$
$\Delta\tilde{x}$ = step size in the streamwise direction
$\Delta\eta_{jj-1}$ = $\eta_j - \eta_{j-1}$ = step size in the cross-stream direction
δ = boundary layer thickness
ε = $\Delta U_e / U_e$ = relative amplitude of the free-stream oscillation
ε_1 = dissipation of turbulent kinetic energy
η = $y/b(x)$ = dimensionless cross-stream co-ordinate
η_B = $y\sqrt{(U_0/2\nu x)}$ = Blasius co-ordinate
η_s = $y\sqrt{(\omega/2\nu)}$ = Stokes co-ordinate in periodic flow
ν = kinematic viscosity of the fluid
ρ = mass density of the fluid
ϕ = phase of the periodic component of U
ω = $2\pi f$ = angular frequency of oscillation
$\langle\ \rangle$ = ensemble-averaged value
overbar = time-averaged value
$\sim$ = ensemble-averaged dimensionless variable

Subscripts

e = edge of boundary layer
0 = upstream value

REFERENCES

1. G. G. Stokes, 'On the effect of the internal friction of fluids on the motion of pendulums', *Math. and Phys. Papers*, III, Cambridge, 1–141 (1901).
2. Lord Rayleigh, 'On the motion of solid bodies through viscous liquid', *Phil. Mag.*, **21,** 697–711 (1911).
3. M. J. Lighthill, 'The response of laminar skin friction and heat transfer to fluctuations in the stream velocity', *Proc. Roy. Soc.*, **224A,** 1–23 (1954).
4. S. Uchida, 'The pulsating viscous flow superposed on the steady motion of incompressible fluid in a circular pipe', *ZAMP*, **7,** 403–421 (1956).
5. P. G. Hill and A. H. Stenning, 'Laminar boundary layers in oscillatory flow', *J. Basic Eng.*, **82,** 593–608 (1960).
6. R. C. Ackerberg and J. H. Phillips, 'The unsteady laminar boundary layer on a semi-infinite plate due to small fluctuations in the magnitude of the free-stream velocity', *J. Fluid Mech.*, **51,** 137–157 (1972).

7. T. J. Pedley, 'Two-dimensional boundary layer in a freestream which oscillates without reversing', *J. Fluid Mech.*, **55,** 359–383 (1972).
8. W. J. McCroskey and J.J. Philippe, 'Unsteady viscous flow on oscillating airfoils', *AIAA Journal*, **13,** 71–79 (1975).
9. T. Cebeci, 'Calculation of unsteady two-dimensional laminar and turbulent boundary layers with fluctuations in external velocity', *Proc. Roy. Soc.*, **355A,** 225–238 (1977).
10. D. Th. Tsahalis and D. P. Telionis, 'Oscillating boundary layers with large amplitude', in F. O. Carta (Ed.) *Unsteady Flows in Jet Engines*, 1974.
11. J. F. Nash and V. C. Patel, '*Three-dimensional turbulent boundary layers*', Scientific and Business Consultants, Inc., Atlanta, 1972.
12. J. Cousteix, R. Houdeville and A. Desopper, 'Resultats experimentaux et methodes de calcul relatifs aux couches limites turbulentes en ecoulement instationnaire', *ONERA T. P. No. 1977, 134* (1977).
13. P. Orlandi, 'Unsteady adverse pressure gradient turbulent boundary layers', R. Michel, J. Cousteix and R. Houdeville (Eds), *Unsteady Turbulent Shear Flows*, Springer-Verlag, Berlin, 1981, pp. 159–170.
14. P. Orlandi and J. H. Ferziger, 'Implicit noniterative schemes for unsteady boundary layers', *AIAA Journal*, **19,** 1408–1414 (1981).
15. J. D. Murphy and P. M. Prenter, 'A hybrid computing scheme for unsteady turbulent boundary layers', *Proceedings of the Third Symposium on Turbulent Shear Flows*, Davis, 8.26–8.34 (1981).
16. A. P. Oskolkov, 'Certain finite-difference schemes for equations of the nonstationary laminar boundary layer', *Foreign Technology Division, FTD-ID (RS)T-0880-77*, 1977.
17. A. N. Menendez and B. R. Ramaprian, 'Calculation of unsteady boundary layers', *IIHR Report No. 248*, 1982.
18. L. Howarth, 'On the solution of the laminar boundary layer equations', *Proc. Roy. Soc.*, **164A,** 547–579 (1938).
19. M. Acharya and W. C. Reynolds, 'Measurements and predictions of a fully developed turbulent channel flow with imposed controlled oscillations', *Stanford University Technical Report TF-8*, 1975.
20. S. W. Tu and B. R. Ramaprian, 'Quasi-steady modelling of periodic turbulent pipe flow', to appear in *AIAA Journal.*
21. P. G. Parikh, W. C. Reynolds and R. Jayaraman, 'Behavior of an unsteady turbulent boundary layer', *AIAA Journal*, **20,** 769–775 (1982).
22. S. V. Patankar and D. B. Spalding, *Heat and Mass Transfer in Boundary Layers*, Morgan-Grampian, London, 1967.
23. F. M. White, *Viscous Fluid Flow*, McGraw-Hill, New York, 1974.